

Luminescence

Highly Luminescence Anthracene Derivatives as Promising Materials for OLED Applications

Aneta Slodek,^[a] Michal Filapek,^[a] Ewa Schab-Balcerzak,^[a,b] Marzena Grucela,^[b] Sonia Kotowicz,^[a] Henryk Janeczek,^[b] Karolina Smolarek,^[c] Sebastian Mackowski,^[c] Jan Grzegorz Malecki,^[a] Agnieszka Jedrzejowska,^[d] Grazyna Szafraniec-Gorol,^[a] Anna Chrobok,^[e] Beata Marcol,^[a] Stanislaw Krompiec,^[a] and Marek Matussek^{*[a]}

Abstract: Novel symmetrical anthracene derivatives with bulky carbazolyl-fluorene, diphenylamino-fluorene, or carbazolyl-carbazole units connected to the anthracene frame through an ethynyl bridge were synthesized in excellent yield by using Sonogashira cross-coupling. The ethynyl bridge in the anthracene dyes increases π -electron conjugation and the bulky substituents considerably attenuate intermolecular interactions. The dyes possess high thermal stability, tremendous solubility in common organic solvents, and especially high photolumines-

cence quantum yield (Φ_f) in solution in the range of 77–98 %. OLED devices were fabricated. The AFM images of thin films and blends prepared from all compounds show a uniform and flat surface, indicating excellent film-forming properties. Devices incorporating the anthracene derivative with diphenylamino-fluorene end-capping groups exhibited the highest value of current density (J). All of the fabricated OLED devices emitted yellowish-orange light under applied voltage.

Introduction

Research on the construction of the organic light-emitting diodes (OLEDs) published in the second half of the twentieth century by Tang and VanSlyke became the prototype for current electroluminescent materials.^[1] The dynamic development of organic electronics, particularly organic light-emitting diodes, is driven by their increasingly impressive performance as a new generation of flexible and low-cost flat-panel displays.^[2,3] The immense achievements in the field of OLEDs can be ascribed to their high efficiency and thermal stability, low power consumption, realistic color reproduction and high transparency.^[4] The emitting materials possess suitable emission with a wide range of colors, high thermal stability and tremendous efficiency, which are desirable characteristics of OLEDs for the development for flat-panel displays.

A number of blue OLEDs based on small molecules with excellent electroluminescence (EL) performance, high efficiency and thermal stability have been reported.^[5–7] In spite of this progress, organic EL devices based on blue-emitters exhibit lifetimes that are rather too short to be marketable; therefore, further efforts in this field with respect to increasing efficiency and color purity have to be made. Indeed, the green and red emitters demonstrate superior color purity, lifetime and efficiency compared with blue emitters.^[8] Luminous efficiency of green and red anthracene-based emitters have been reported to be as high as 20 and 8.5 cd/A, respectively.^[9,10]

Anthracene and its derivatives have been extensively investigated for many years especially as blue-light emitters. The derivatives have attracted attention as small organic molecules possessing unconventional physical properties, such as outstanding electroluminescence and photoluminescence (PL), high thermal stability, and extensive conjugated π -electron structure.^[11] In addition, anthracene derivatives are stable compounds that are amenable for substitution at the 9- and 10-positions. Modifications of anthracene with bulky groups along with a great variety of electron-donating (D) and electron-withdrawing (A) substituents is of particular importance for suppressing aggregation by steric hindrance, improvement the EL performance, and enhancement of π -conjugated structure.^[12] Fluorene,^[13,14] carbazole,^[15,16] naphthalene,^[17] and tri(phenyl)silane^[18] derivatives are often selected as blue-emitting building blocks for synthesis of anthracene-based emitters. A number of D-A-D, D- π -A, D- π -A- π -D compounds based on the anthracene frame have been reported.^[19–22] Recently, D-A-D molecules based on anthracene with bulky moieties, namely 9,10-bis(9',9'-diethyl-7'-diphenylamino-fluorene-2-yl)anthracene

[a] Faculty of Mathematics, Physics and Chemistry, Institute of Chemistry, University of Silesia, Szkolna 9, Katowice, 40-007, Poland
E-mail: matussekmarek@gmail.com
http://inorganic.us.edu.pl

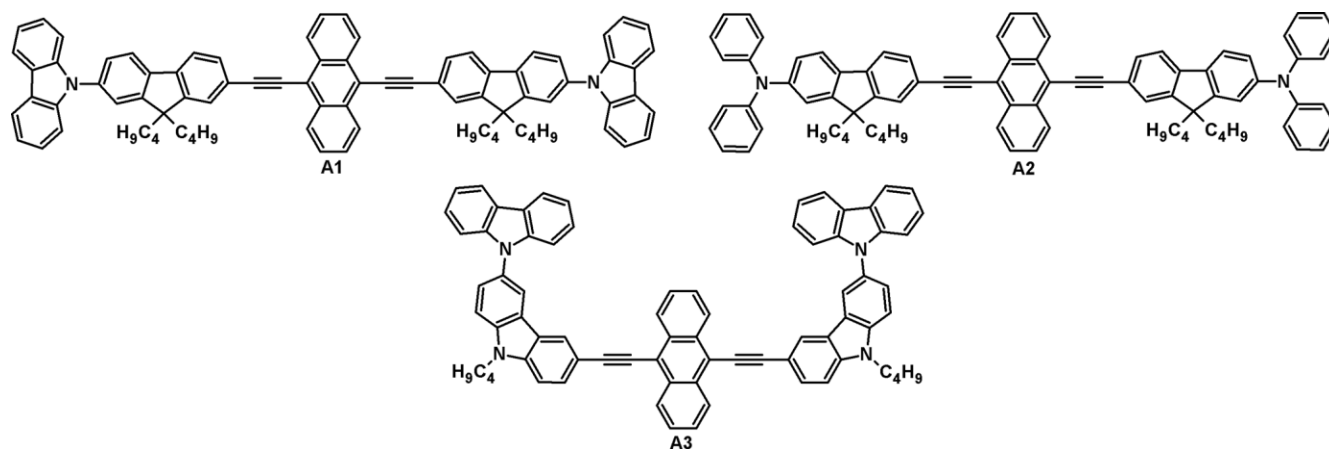
[b] Centre of Polymer and Carbon Materials, Polish Academy of Sciences, M. Curie-Skłodowska 34, Zabrze, 41-819, Poland

[c] Institute of Physics, Faculty of Physics, Astronomy and Informatics, Nicolaus Copernicus University, Grudziadzka 5, Torun, 87-100, Poland

[d] Faculty of Mathematics, Physics and Chemistry, Institute of Physics, University of Silesia, Uniwersytecka 4, Katowice, 40-007, Poland

[e] Department of Chemical Organic Technology and Petrochemistry, Silesian University of Technology, Krzywoustego 4, Gliwice, 44-100, Poland

Supporting information for this article is available on the WWW under <http://dx.doi.org/10.1002/ejoc.201600532>.

Figure 1. Structure of dyes **A1–A3**.

(BDDFA) were synthesized and studied as blue-light emitting material in OLED, showing high quantum efficiency of 3.3 % with maximum brightness of 4200 cd/m².^[23] A maximum current efficiency of 3.6 cd/A was achieved for an EL device with a D-A-D framework based on the anthracene scaffold combined with naphthalene moieties. It was observed that the introduction of substituents in the 2-position of the anthracene leads to a non-coplanar structure and suppression of the intermolecular interactions, which results in high efficiency and color purity for blue-light emitting materials.^[24]

In this study, we present the synthesis and comprehensive characterization of orange-emitting materials based on symmetrically substituted anthracene of D- π -A- π -D type, 9,10-bis[[7-(9*H*-carbazol-9-yl)-9,9-dibutylfluoren-2-yl]ethynyl]anthracene (**A1**), 9,10-bis[[7-(*N,N*-diphenylamino)-9,9-dibutylfluoren-2-yl]ethynyl]anthracene (**A2**), and 9,10-bis[[6-(9*H*-carbazol-9-yl)-9-butylcarbazol-3-yl]ethynyl]anthracene (**A3**) (Figure 1). In these D- π -A- π -D molecules, anthracene, acting as the acceptor, is connected with donating moieties, such as carbazole or fluorene, through triple bonds (C \equiv C). The use of the triple bond as the conjugated bridge between building blocks (D, A) ensures lack of torsion, providing planarity of the molecule, which significantly increases π -electron conjugation. In addition, the bulky carbazolyl-fluorene, diphenylamino-fluorene, and carbazolyl-carbazole groups in novel orange emitters, significantly suppress intermolecular interactions and yield high quantum efficiency and high stability. The synthesis of novel compounds **A1–A3** was developed, and a detailed electrochemical, photo-physical, theoretical, and electrical characterization of the dyes was undertaken.

Results and Discussion

Synthesis

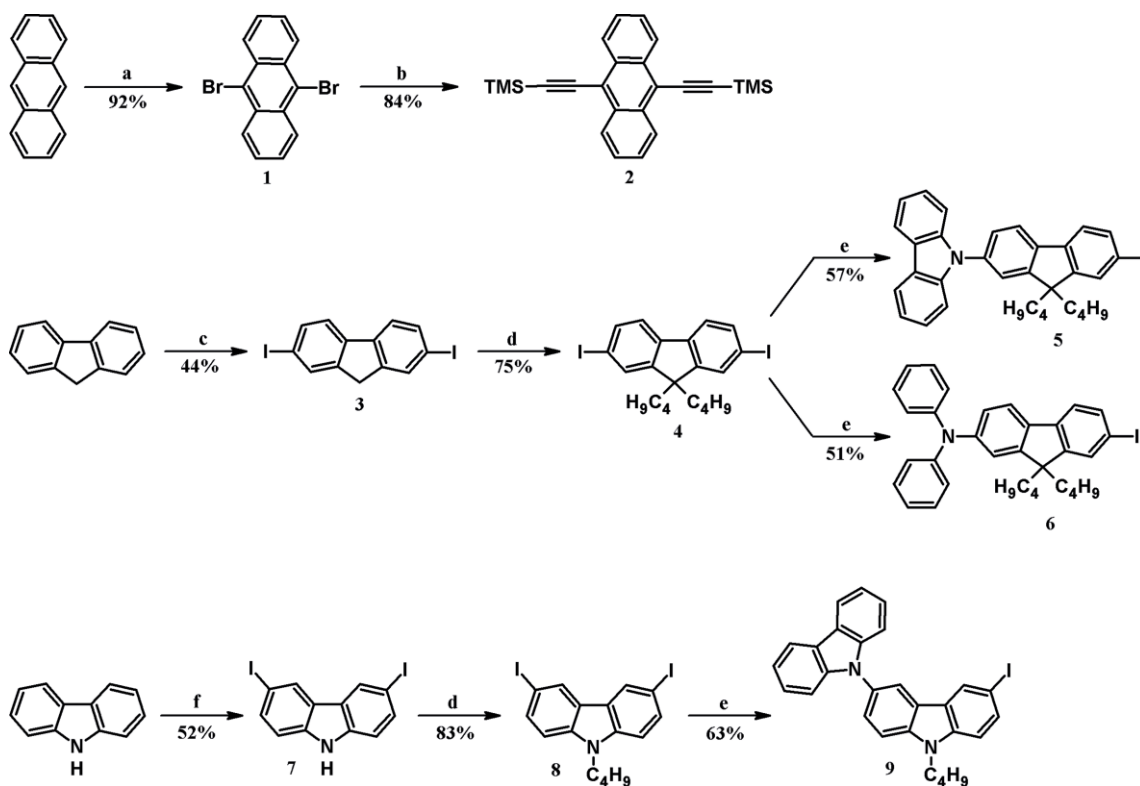
The structures of designed anthracene derivatives **A1–A3** are presented in Figure 1. Scheme 1 illustrates the routes used for the synthesis of intermediates **1–9**, which were required for the preparation of target compounds **A1–A3** (Scheme 2). The key intermediates were synthesized according to well-known proce-

dures with minor modifications, which resulted in higher yields. In the first step, anthracene was brominated at the 9- and 10-positions to give **1** in 92 % yield. The latter was then converted into protected (ethynyl)anthracene derivative **2** through Sonogashira coupling reaction with trimethylsilylacetylene (TMSA) in the presence of CuI and Pd(PPh₃)₄. Iodoarenes **5** and **6** were obtained from commercially available fluorene upon iodination, followed by alkylation under conditions of phase-transfer catalysis (PTC) to afford 2,7-diiodo-9,9-dibutylfluorene **4** in 75 % yield. Ullmann condensation of **4** with either carbazole or diphenylamine, resulted in the formation of target intermediates **5** and **6**, respectively. Iodoarene **9** was synthesized by following procedures similar to those used for **5** and **6**. Briefly, iodination of carbazole gave **7**, then *N*-alkylation afforded 9-butyl-3,6-diiodocarbazole **8** in 83 % yield, and finally Ullmann condensation of **8** provided **9** in 63 % yield.

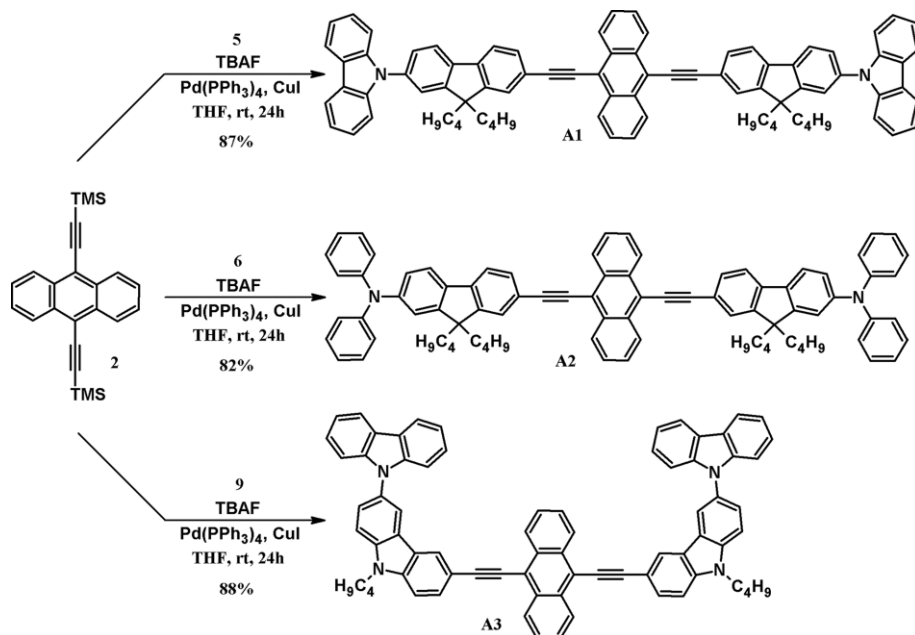
The desired anthracene derivatives **A1–A3** were prepared by prior deprotection of 9,10-bis(trimethylsilyl)ethynyl]anthracene **2** by treatment with tetrabutylammonium fluoride (TBAF), and followed by Pd-catalyzed Sonogashira cross-coupling reaction in situ with the respective iodoarene **5**, **6**, or **9** (Scheme 2). The synthesis of a compound similar to **A1** but with a longer alkyl chain (*n*-hexyl) at the 9,9'-position of the fluorene has recently been described and examined as a dye applied in two-photon excited fluorescence.^[25] However, 9,10-bis[[7-(9*H*-carbazol-9-yl)-9,9-dihexyl-9*H*-fluoren-2-yl]ethynyl]anthracene was prepared by using a different synthetic route with 67 % yield.

The target compounds were obtained as orange (**A1**), red (**A2**), and brown (**A3**) solids (Figure 2) with high yields in the range of 82–88 %. Our design of D- π -A- π -D type molecules based on anthracene derivatives bearing fluorene, carbazole, and diphenylamine moieties with high π -electron linkage was developed to achieve highly π -conjugated systems.

In addition, triple (C \equiv C) bonds as linkage between building blocks (D and A) prevents torsions, and primarily allows for a free rotation of D and A fragments leading to a planarity of the molecule (Figure 3).^[26] The obtained compounds **A1–A3** were fully characterized by standard spectroscopic methods (¹H and ¹³C NMR, mass spectrometry). The chemical structures of the synthesized compounds were also confirmed based on elemen-



Scheme 1. Synthesis of compounds **1–9**. Reagents and conditions: (a) Br₂, CHCl₃, room temp., 4 h; (b) TMSA, Pd(PPh₃)₄, CuI, THF/TEA, 60 °C, 24 h; (c) I₂, H₅IO₆, AcOH/H₂O/H₂SO₄, 70 °C, 6 h; (d) 50 % NaOH, TBAB, *n*-C₄H₉Br, DMSO, room temp., 8 h; (e) carbazole (for **5**, **9**) or diphenylamine (for **6**), CuI, K₂CO₃, 1,10-phenanthroline, DMF, reflux, 30 h; (f) KI, KIO₃, AcOH, reflux, 15 min.



Scheme 2. Synthetic route for the preparation of **A1–A3**.

tal analysis, which showed good agreement between the calculated and experimentally determined carbon, nitrogen, and hydrogen content. However, a deficiency in the carbon content of about 1 % was found, which is likely a result of the difficulties in burning these high-temperature compounds, which was also

observed for other thermostable materials.^[27] To verify this assumption, DSC measurements were performed to assess the purity of the compounds. As expected, high purity of anthracene derivatives **A1** and **A2** (above 98 %) was confirmed by using this technique (see the Experimental Section). Moreover,



Figure 2. Form (powders) of the target compounds.

all compounds exhibit excellent solubility in common organic solvents, such as acetone, dichloromethane, chloroform, ethyl acetate or tetrahydrofuran, which allows the easy fabrication of devices.

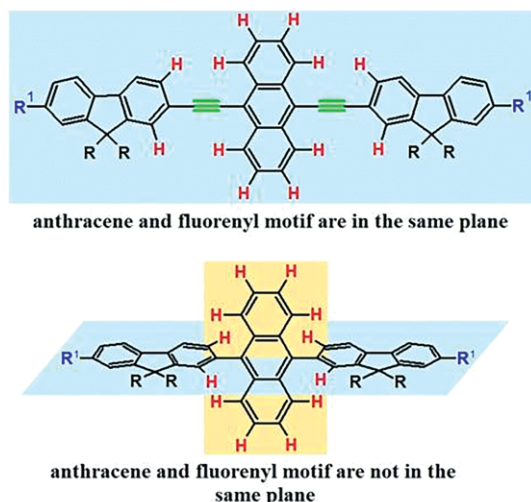


Figure 3. The approach of using a linkage, which influences on the geometry of molecules.

Thermal Properties

The thermal properties of the investigated compounds were evaluated by differential scanning calorimetry (DSC) and thermogravimetric analysis (TGA) under nitrogen atmosphere; the obtained results are shown in Table 1.

Table 1. Thermal properties of the anthracene derivatives.

	TGA			DSC	
	$T_{5\%}^{[a]}$ [°C]	$T_{10\%}^{[a]}$ [°C]	Char yield ^[b] [%]	T_g [°C]	T_m [°C]
A1	434	460	58	185	301
A2	402	433	48	124	286
A3	478	512	70	133	–

[a] $T_{5\%}$, $T_{10\%}$: temperatures at 5, 10 % weight loss, respectively. [b] Residual weight when heated to 800 °C in nitrogen.

Based on the DSC results, it was found that the investigated anthracene derivatives can form stable amorphous glasses above room temperature; thus, they belong to a class of organic functional materials referred to as molecular glasses, which has attracted increasing attention since the development of organic optoelectronic devices.^[28] They possess many valuable proper-

ties, including the ability to form uniform, transparent amorphous thin layers by vapor deposition and spin-coating methods, in contrast to single crystals and liquid crystals.^[29] When crystalline samples of anthracene derivatives **A1** and **A2**, obtained after purification, were heated, an endothermic peak due to melting was observed. When the isotropic liquid was cooled, in their 2nd heating DSC scan, the thermograms display an endothermic baseline shift owing a glass transition (T_g) phenomenon. Additionally, in the case of **A2**, upon further heating beyond T_g an exothermal crystallization was found at 182 °C, and subsequent melting was observed at 284 °C. Figure 4 shows DSC thermograms of **A2**.

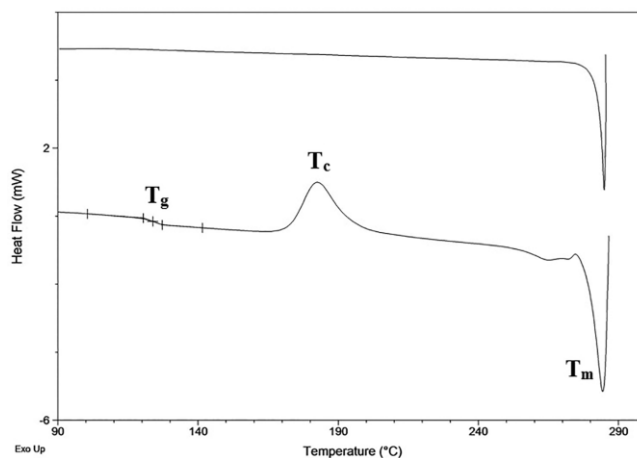


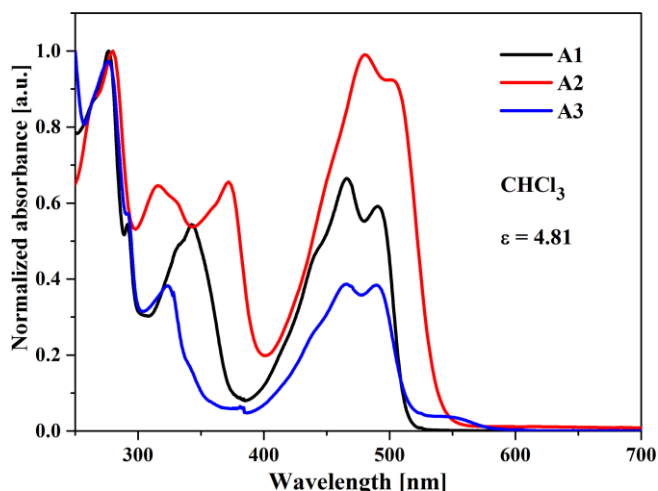
Figure 4. DSC thermogram of **A2**. T_g – glass transition temperature; T_c – crystallization temperature; T_m – melting point temperature.

In the case of **A3**, without dibutylfluorene units, only T_g was observed during heating scans. The highest T_g was observed for **A1**, with dibutylfluorene end-capped with carbazole units. The TGA results showed that all molecules retain high thermal stability, with decomposition temperatures corresponding to 5 % weight loss ($T_{5\%}$) over 400 °C.

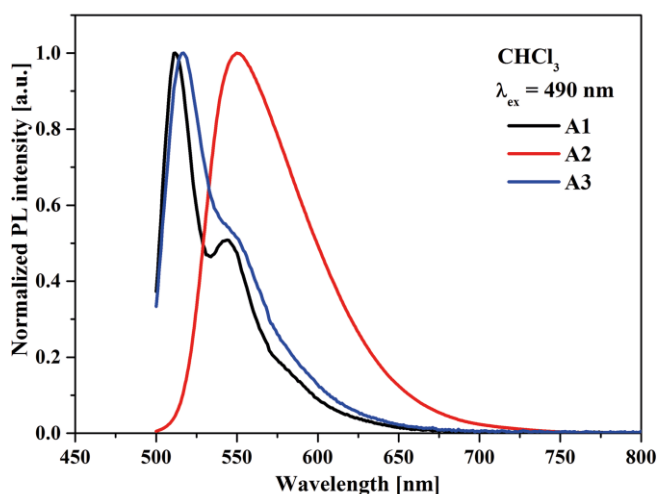
Photophysical Properties

The photophysical properties of anthracene derivatives were investigated by UV/Vis spectroscopy and photoluminescence (PL) measurements carried out in chloroform solution (Figure 5), and in solid state, both as a film and blended with poly(9-vinylcarbazole) (PVK). The obtained data are collected in Table 2 and UV/Vis spectra of compound **A1** are presented in Figure 6.

Electronic spectra of the studied anthracene derivatives (except for **A2**) exhibited similar characteristics with several bands between 250 and 600 nm (Figure 5, a). The first, most intense band is observed below 300 nm. Differences in absorption in the range 300–400 nm are seen for **A2** and the other two compounds. Compound **A2** exhibited two bands with maxima (λ_{max}) at 316 and 372 nm, whereas **A1** and **A3** showed one band with λ_{max} at 342 and 322 nm, respectively. The pronounced differences result from the chemical structure of the compounds. Compounds **A1** and **A3** are similar because they are both end-capped with carbazole derivative, whereas **A2** contains diphenylamine units as end group. For the UV/Vis



(a)



(b)

Figure 5. (a) The UV/Vis and (b) PL spectra of **A1–A3** in chloroform solution ($c = 10^{-5}$ mol/L).

properties of intermediate compounds **5** (corresponds **A1**) and **6** (corresponds **A2**), the same differences are found. In the UV/Vis spectrum of **5** above 300 nm, one absorption with λ_{max} at 326 nm is detected, in contrast to **6**, which exhibited two λ_{max} at 311 and 357 nm. The presence of these bands is also seen in the final compounds **A2** and **A1**; however, their maxima are slightly shifted because of changes in their electronic environ-

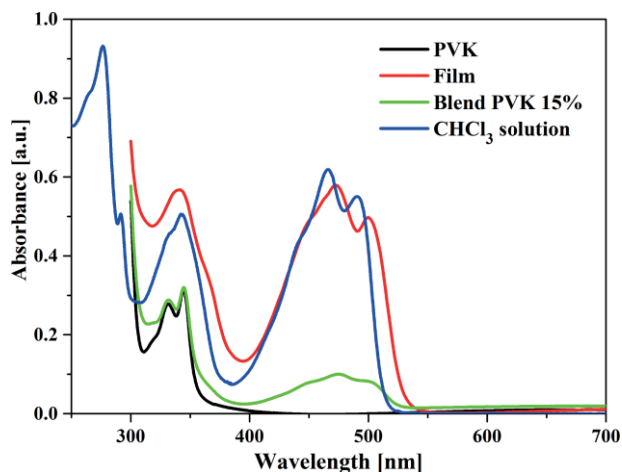


Figure 6. The UV/Vis spectra of **A1** in chloroform solution ($c = 10^{-5}$ mol/L) and in solid state together with PVK spectrum in film.

ment by the introduction of the anthracene unit. Above 400 nm, compounds **A1–A3** all have similar vibration patterns of absorption band connected with the presence of the anthracene structure. The absorption spectra of the anthracene derivatives in the solid state revealed a slight bathochromic shift of the absorption band maximum with respect to that in solution.

The emission spectra of studied compounds were measured in chloroform solution under different excitation wavelengths (Figure 5, b). The influence of the excitation wavelength (λ_{ex}) on PL properties is exemplified for compound **A1** in Figure 7.

Changes in the emission intensity with an increase of λ_{ex} from 300 to 500 nm were observed. The investigated anthracene derivatives under different excitation wavelengths exhibited a single emission band with vibronic pattern in the case of **A1** and **A3**, and the maximum of the emission is located in the green spectral region. The most intense emission of light was found under excitation at $\lambda_{\text{ex}} = 490$ nm. Compounds **A1–A3** emitted light in chloroform solution with very high PL quantum yields (Φ_f) in the range of 98–77 % (Table 2), suggesting that they would have highly efficient electroluminescent properties in OLED devices. Compound **A3**, which does not contain dibutylfluorene units, exhibited the lowest Φ_f . Probably, the molecular structure of the anthracene derivatives possesses a relatively high rigidity, which promotes a high PL efficiency. Considering the rigidity of these compounds, it seems that the highest and the lowest Φ_f should be observed in the case of

Table 2. UV/Vis and PL data of investigated compounds in solution, film, and blend.

	Medium	UV/Vis (ϵ [L·mol ⁻¹ cm ⁻¹]) λ_{max} [nm]	PL λ_{em} [nm] $\lambda_{\text{ex}} = 490$ nm	Φ_f ^[d]
A1	solution ^[a]	276 (91,136); 292 (49,530); 342 (51512); 466 (60,427); 490 (55,474)	511; 544	0.93
	film	368; 472; 500	529; 560	0.10
	blend ^[b]	330; 345; 473; 500 ^[c]	521; 553	0.01
A2	solution ^[a]	262 ^[c] ; 280 (144,273); 316 (92,955); 372 (93,923); 480 (143,305); 502 (133,622)	548	0.98
	film	314; 375; 473; 536	556; 586 ^[c]	0.11
	blend ^[b]	331; 343; 372; 484	562	0.15
A3	solution ^[a]	276 (102,984); 322 (39,766); 465 (38,746); 489 (37,727)	517; 550	0.77
	film	330; 477; 504; 554 ^[c]	640	0.17
	blend ^[b]	330; 345; 476; 500 ^[c]	589	0.11

[a] CHCl₃; $c = 10^{-5}$ mol/L. [b] 15 wt.-% content of compound in PVK. [c] The second-derivatives method was used to find the position. [d] Φ_f – quantum yield.

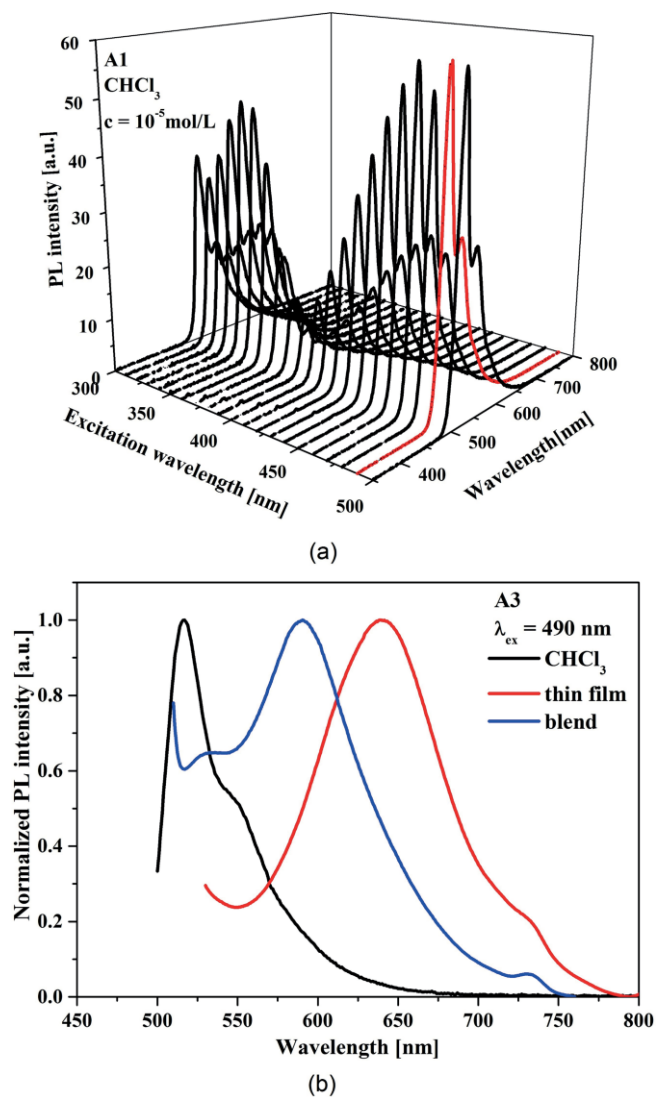


Figure 7. (a) The effect of λ_{ex} on PL properties of compound **A1** in chloroform solution ($c = 10^{-5}$ mol/L) and (b) PL spectra of **A3** in solution and in the solid state.

compounds **A3** and **A2**, respectively. Dynamic intramolecular rotation of diphenylamine derivatives in **A2** may cause nonradiative reduction of its excited states leading to lower Φ_f . In the presented compounds the opposite trend was found. However, to confirm the molecule rigidity, calculations of the bond rotational barrier and comparison with results from X-ray measurements are necessary. Moreover, other phenomena may influence the PL intensity, such as photoinduced electron transfer (PET) and intersystem crossing (ISC).

In the PL spectra of the blends, the emission band coming from the anthracene derivative dominates the spectra. The emission spectra of **A1–A3** in blend with PVK revealed that the λ_{em} was bathochromically shifted with respect to the chloroform solution. The same tendency, that is, shift of λ_{em} to lower energetic region, was found for the compounds in the form of film on glass substrate (Table 2 and Figure 7, b). This redshift of the λ_{em} is probably due to molecular packing. The significant shift of λ_{em} from the green to the orange region was observed

for anthracene derivative **A3**, without dibutylfluorene units. Compound **A2** showed the same position of λ_{em} in solution as in the solid state. However, the emission quantum yield of the samples in the solid state was much lower than those in solution, and the highest Φ_f of about 17% was found for **A3** (Table 2).

Electrochemical Properties

The electrochemical properties of **A1–A3** were investigated in CH_2Cl_2 solution by means of cyclic voltammetry (CV). Representative cyclic voltammograms are presented in Figure 8. The electrochemical oxidation and reduction onset potentials were

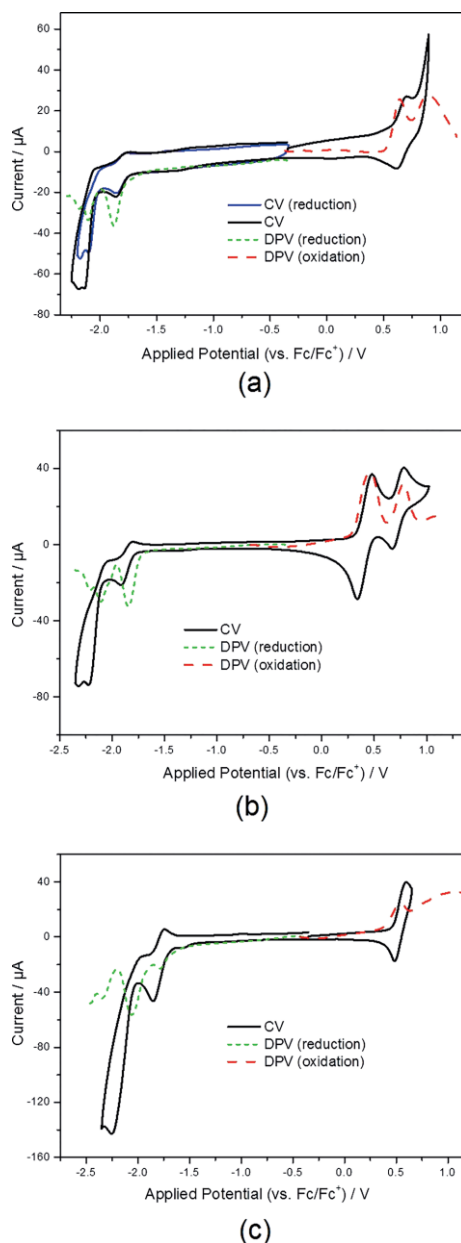


Figure 8. Voltammograms of (a) **A1**, (b) **A2**, and (c) **A3** during reduction and oxidation processes. GC as working electrode; sweep rate $\nu = 100$ mV/s for CV or 2.5 mV/s for DPV measurements, 0.1 M Bu_4NPF_6 in CH_2Cl_2 .

Table 3. Electrochemical data for **A1–A3**.

	$E_{1\text{red}}$ [eV]	$E_{2\text{red}}$ [eV]	$E_{3\text{red}}$ [eV]	$E_{1\text{ox}}$ [eV]	$E_{2\text{ox}}$ [eV]	HOMO ^[a] (CV) (eV)	LUMO ^[b] (CV) (eV)	HOMO (DFT)	LUMO (DFT)	E_g (CV) ^[c] [eV]	E_g (opt) [eV]	E_g (DFT) [eV]
A1	-1.74	-2.03	-2.16	0.56	0.77	-5.66	-3.36	-5.23	-2.75	2.30	2.40	2.48
A2	-1.84	-2.12	-2.28	0.31	0.67	-5.41	-3.26	-5.02	-2.69	2.15	2.29	2.33
A3	-1.82	-2.04	-2.32	0.45	0.72	-5.55	-3.28	-5.59	-2.73	2.27	2.36	2.86

[a] HOMO = $-5.1 - E_{\text{CV ox}}$. [b] LUMO = $-5.1 - E_{\text{CV red}}$. [c] $E_g = E_{\text{ox}}$ (onset) $- E_{\text{red}}$ (onset); 1 mM in CH_2Cl_2 with 0.1 M Bu_4NPF_6 .

used to estimate the HOMO and LUMO energies (or rather, ionization potentials and electron affinities) of the materials (assuming that the IP of ferrocene was -5.1 eV).^[30] The calculated HOMO and LUMO levels together with electrochemical energy band gap (E_g) are presented in Table 3. All compounds have similar properties during the reduction processes. The first reduction step ($E_{1\text{red}}$) (in the range from -1.74 to -1.84 V) is reversible. This is undoubtedly caused by reduction of the anthracene moiety. However, $E_{1\text{red}}$ values differ slightly depending on donor properties of the substituents. Further reduction of the potential allows for registration of two more reduction degrees ($E_{2\text{red}}$ and $E_{3\text{red}}$). For **A1** and **A3**, $E_{2\text{red}}$ is almost equal in the value (i.e., ca. -2.04 V). This observation suggests the reduction of terminal carbazole moieties. In the case of **A2**, $E_{2\text{red}}$ is slightly lower (occurs at -2.12 V), which is a consequence of the strong donating character of the diphenylamine end-capping group.

On the other hand, differences during the oxidation process are significant because oxidation takes place at the π -excess moiety. Thus, higher electron-excising ring character results in higher HOMO energy level (as a consequence, smaller E_{ox} value is observed). Indeed, in the case of **A2** (possessing strong donor – diphenylamine moieties), $E_{1\text{ox}}$ occurs at the lowest potential: 0.31 V. As can be seen in Figure 8, b, $E_{2\text{ox}} = 0.67$ V. It is worth noting that, in both cases, the oxidation is fully reversible. However, the charge accompanying $E_{1\text{ox}}$ is twice as high as measured for $E_{2\text{ox}}$. The first oxidation step probably occurs at the diphenylamine moiety (**A2** possesses two Ph_2N moieties per molecule) and the second at the anthracene moiety. For **A1** and **A3**, only $E_{1\text{ox}}$ is reversible. Additionally, in the case of **A3** (having carbazole end-capping groups), polymerization at potentials higher than $E_{2\text{ox}}$ was observed.

It can be seen in Table 3 that the energy gaps obtained from independent methods (i.e., from cyclic voltammetry, UV/Vis spectroscopy, and DFT calculations) are consistent in tendency. This implies that band gaps, as well as both HOMO and LUMO energy levels, can be tuned conveniently by changing the electron-donating ability of the donor in D- π -A- π -D dyes. However, in each case, the band gaps determined for diluted solutions by UV/Vis spectroscopy are higher than those obtained by using cyclic voltammetry techniques.

Electroluminescence Properties

The synthesized anthracene derivatives exhibited green emission in dilute solution (see the Supporting Information, Figure S7) with high quantum yield, which are expected to serve as emitters in OLEDs. Two kinds of OLEDs were prepared: in the first case, a neat film was used as the emitter layer, and in the second device the active layer was obtained by doping PVK

with 15 wt.% **A1–A3**. All studied compounds have appropriate HOMO and LUMO levels considering the PVK matrix. The HOMO of the guest (in the case of compounds **A1–A3**) is higher than the HOMO level of PVK (PVK HOMO = -5.8 eV) and the LUMO level of anthracene derivatives **A1–A3** is lower than the LUMO of the matrix (PVK LUMO = -2.2 eV). Thus, one of the effective OLED functioning conditions is fulfilled for all investigated compounds (Table 3).

The electroluminescent properties of the synthesized anthracene derivatives were tested in devices with a configuration ITO/PEDOT:PSS/compound/Al and ITO/PEDOT:PSS/blend/Al (thickness of active layer are given in Table 4). The morphol-

Table 4. J–V characteristic parameters of devices based on anthracene derivatives together with electroluminescence wavelength maximum (λ_{EL}) and the thickness and surface roughness (RMS) of the active layer.

	Active layer	J [mA/cm ²]	V_{on} [V]	λ_{EL} [nm]	Thickness [nm]	RMS [nm]
A1	film	0.9	2.6	–	125	1.498
	blend	9.8	–	536; 550	125	0.926
A2	film	2.2	1.8	–	97	0.676
	blend	78.5	–	580	115	1.099
A3	film	0.9	2.6	–	40	2.143
	blend	5.4	–	620	135	1.500

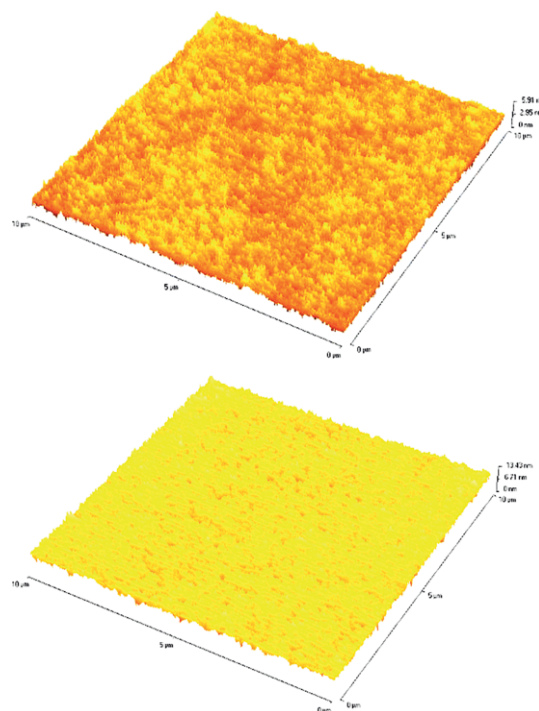


Figure 9. AFM images (10 $\mu\text{m} \times 10 \mu\text{m}$) of **A2** (top) and 15 % doped PVK with **A2** (bottom).

ogy />of the spin-coated films, which is another key factor for the OLED fabrication, was investigated by atomic force microscopy (AFM). Figure 9 presents examples of AFM images for **A2** layer and for a blend of **A2** with PVK. The AFM images of thin films and blends prepared from all compounds show a uniform

and flat surface, indicating excellent film-forming properties. The surface root-mean-square roughness (RMS) of these layers were in the range of 0.676–2.143 nm.

For the fabricated OLED devices, current density-voltage (J - V) characteristics were registered. Figure 10 presents an example of the J - V characteristics for compound **A3**; the data obtained for all devices are collected in Table 4.

The turn-on voltage (V_{on}) of the devices based on compound end-capped with diphenylamine units **A2** was lower than those of other anthracene derivatives. Additionally, the devices with this compound achieved the highest value of current density (J). OLEDs prepared by using neat film of anthracene derivatives exhibited lower J values in relation to devices in which the active layer was a blend. All fabricated devices emitted yellowish-orange light under the applied voltage (Figure 10). For the devices based on PVK doped with anthracene derivatives, the electroluminescence (EL) spectra were registered (Figure 11).

The EL spectra of devices were found to have emission with maximum wavelength (λ_{El}) between 550 and 620 nm. The EL spectra measured for all three compounds correspond well to the photoluminescence spectra and the bathochromic shifts of λ_{El} in the range of 15–31 nm compared with its PL spectra in the blend were seen. In addition, the signal measured for the diode with anthracene derivative **A1** exhibited a bimodal character, similar to that of the PL band. As shown in Figure 11, in

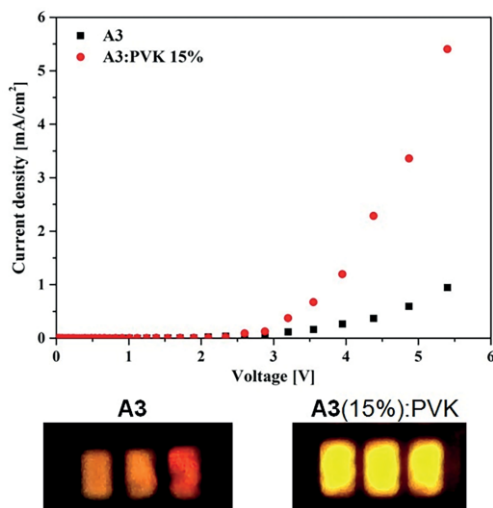


Figure 10. J - V characteristics of the **A3**-based devices together with images of the fabricated devices.

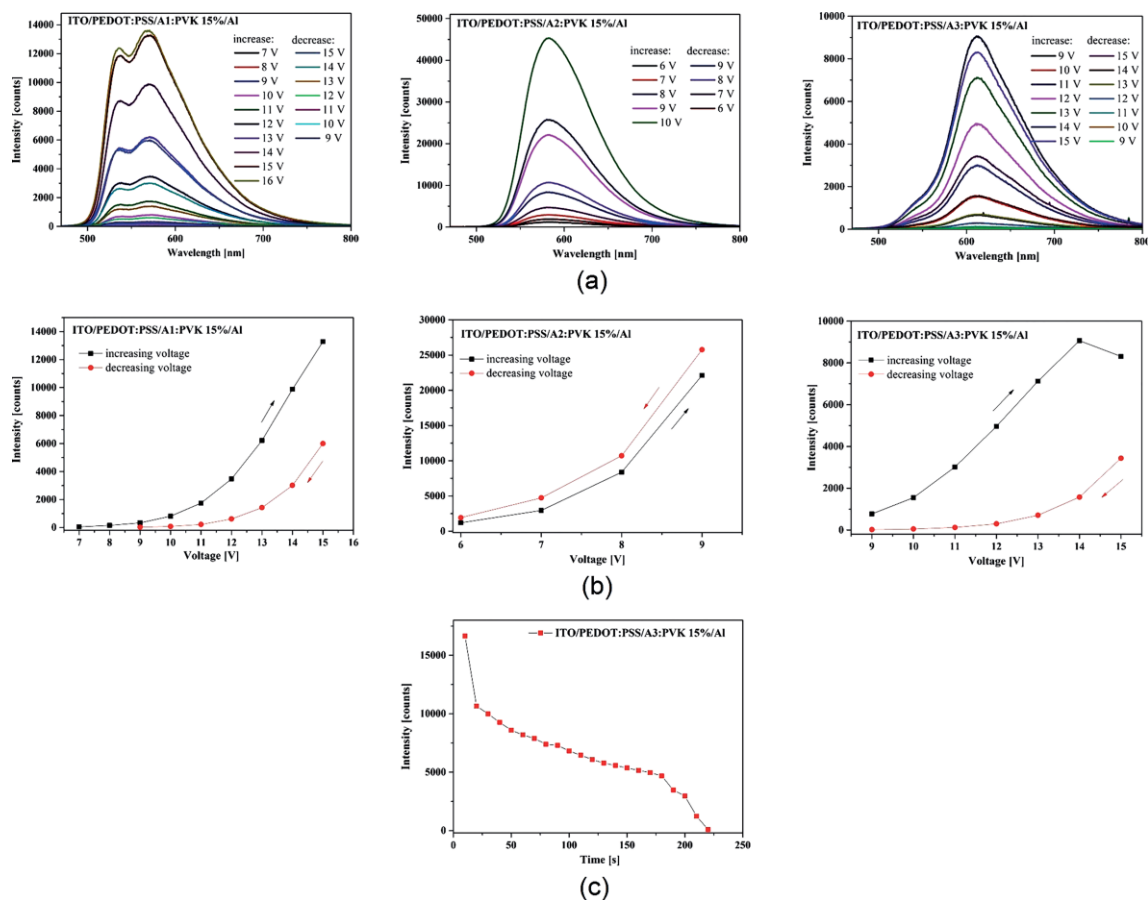


Figure 11. (a) Electroluminescence spectra of fabricated OLEDs for increasing and decreasing external voltages, (b) EL intensity as a function of voltage for the investigated OLEDs and (c) EL intensity as a function of time for ITO/PEDOT:PSS/**A3**:PVK 15% structure under an external voltage of 20 V.

all cases, the emergence of emission was observed between 7 and 9V applied voltage. No variation of the EL spectra as a function of the external voltage for a given structure was found, which points towards the stability of the electronic properties. The intensities of EL are the highest in the case of the ITO/PEDOT:PSS/**A2**:PVK 15 % structure. In addition, in the case of the structure based on **A3**, temporal behavior of the EL signal for the external voltage of 20 V was also measured (Figure 11, c). The experiment carried out at a fixed external voltage as a function of time reveals that the investigated device exhibits modest stability, with the signal diminishing after 3 minutes. Clearly, further work towards the protection of such devices is required.

It should be noted that the OLEDs presented in this work have a simple structure because the aim was to investigate the ability of the synthesized materials to electroluminesce. Clearly, device performance could be improved by the introduction of additional charge transporting layers, such as carrier injection and charge transport layers.

DFT Calculations

To gain further insight into the optical and electronic properties of the anthracene derivatives **A1–A3**, quantum theoretical calculations at the density functional theory level were performed. Based on the optimized geometries, the energy and electronic distribution of molecular frontier orbitals were calculated in dichloromethane for comparison with experimental (electrochemical) potentials. Three-dimensional plots of the electron density for the HOMO and the LUMO of **A1–A3** are shown in Figure 12, whereas the orbital energies and compositions are summarized in Table S1 (see the Supporting Information). Moreover, the partial density of states diagrams are also included (see the Supporting Information, Figure S8). The molecule of each compound was divided into three fragments such as: -CC-anthracene-CC-, fluorene-(C₄H₉)₂, carbazole, Ph₂N-, respectively, and their contribution to each molecular orbital was calculated. The electronic structures of **A1** and **A3** are similar and the HOMO and LUMO in both cases are localized mainly on the anthracene-ethynyl moiety with some participation of the fluorene-(C₄H₉)₂ **A1** or carbazole-C₄H₉ **A3** orbitals (Table S1). The character of the HOMO and LUMO can be defined as nonbonding (n) and π^* antibonding, respectively (Fig-

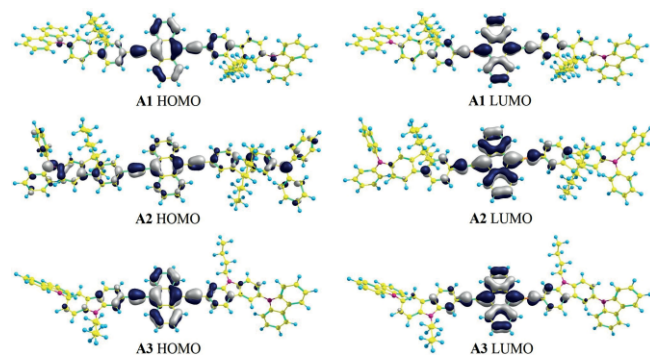


Figure 12. Contours of HOMOs and LUMOs of **A1–A3**.

ure 12). In the case of **A2**, the HOMO comprises the whole molecule, whereas the LUMO is localized on the -CC-anthracene-CC- fragment with some contribution of fluorene-(C₄H₉)₂, as seen in Figure 12 and Table S1.

The calculated HOMO and LUMO energies are close to the values determined from electrochemical measurements, although the energies of LUMO are higher than the experimental values. The virtual orbitals are generally more difficult to describe theoretically than the occupied orbitals, and the errors in the LUMO eigenvalues are also usually significantly larger, with the calculated LUMO eigenvalues being much higher in energy than those determined experimentally.

The dichloromethane solutions of **A1–A3** reveal photoluminescence excited at 488 (**A1**, **A3**) and 498 nm (**A2**). The electronic absorption spectra of **A1–A3** were calculated by using the CIS(D) method with CH₂Cl₂ as solvent in the polarizable continuous model (PCM). Selected electronic transitions assigned to the excitation wavelengths are collected in Table 5. Taking into account the electronic structures of the compounds, the luminescence active transitions have mixed $\pi \rightarrow \pi^*/n \rightarrow \pi^*$ character. Moreover, considering the molecular orbitals involved in electronic transitions, it can be assumed that the excitation processes have intramolecular charge transfer (ICT) character. In **A1**, ICT occurs between fluorene-(C₄H₉)₂ and anthracene-ethynyl fragments, in **A3** between carbazole-C₄H₉ and anthracene, and in the case of **A2**, fluorene-(C₄H₉)₂ and anthracene-ethynyl moieties play the acceptor role. The Stokes shift of **A1** and **A3** are similar and about two times smaller than for **A2**. The smaller bathochromic shift observed for **A1** and **A3** may be due to their rigid structure (the nuclear structure of the molecule does not substantially deviate from its Franck–Condon geometry), which enhances the intramolecular energy transfer process. In the case of **A2**, the greater nuclear geometry distortion with respect to the ground state results in a larger shift of the emission maximum.

Table 5. Selected electronic transitions calculated for CH₂Cl₂ solutions of **A1–A3**.

	λ_{ex}	λ_{calc} (f)	Transition	Character ^[a]
A1	488	489.7 (0.011)	H-5→LUMO (47 %)	$\pi_{\text{flu}} \rightarrow \pi^*_{\text{anth}}$
			HOMO→L+1 (52 %)	$n_{\text{anth}} \rightarrow \pi^*_{\text{flu}}$
A2	498	496.1 (0.0251)	H-3→LUMO (13 %),	$\pi \rightarrow \pi^*_{\text{anth}}$
			H-1→L+2 (15 %)	$\pi_{\text{Ph2N}} \rightarrow \pi^*_{\text{flu}}$
			HOMO→L+1 (71 %)	$\pi \rightarrow \pi^*_{\text{flu}}$
A3	488	484.7 (0.0175)	H-7→LUMO (65 %)	$\pi_{\text{carb-C4H9}} \rightarrow \pi^*_{\text{anth}}$
			HOMO→L+1 (33 %)	$n_{\text{anth}} \rightarrow \pi^*_{\text{carb-C4H9}}$

[a] flu, anth, carb denote respectively fluorene, -CC-anthracene-CC- and carbazole subunits.

Conclusions

We have presented the synthesis and comprehensive characterization of novel symmetrically substituted anthracene derivatives of D- π -A- π -D type: **A1**, **A2**, and **A3**, where anthracene, acting as acceptor (A), is connected to donating moieties, such as carbazolyl-fluorene, diphenylamino-fluorene, carbazolyl-carbazole groups through triple bonds. The novel anthracene derivatives **A1–A3** were prepared by Sonogashira cross-cou-

pling with excellent yield in the range of 82–88 %. The novel compounds are yellowish-orange emitters with high thermal stability and excellent solubility in most organic solvents. Cyclic voltammetry of all studied compounds reveals that all of them undergo multistep oxidation and reduction, with fully reversible first step of these processes. The values of band gaps obtained electrochemically, optically, and by DFT are very similar. This result implies that changes to the donor part in anthracene derivatives **A1–A3** might be used as a convenient way to tune the band gap, as well as to adjust both HOMO and LUMO energy levels.

It should be stressed that the synthesized anthracene derivatives fulfill the key requirements for organic electroluminescence devices, including (1) suitable ionization potentials and electron affinity for energy level fitting for the injection of charge carriers at the interfaces between the electrode/organic material and organic material/organic material, (2) the ability to form uniform films, (3) thermal and electrochemical stability and (4) high PL quantum yield in CH₂Cl₂ solution ranging from 77 to 98 %. These compounds show electroluminescence response and emission of yellowish-orange light at forward applied voltage. The highest intensities of EL were observed for OLED devices based on compounds with end-capped diphenylamine units.

Experimental Section

Materials: All reagents were of analytical reagent grade, and were used without further purification. Solvents were distilled by using standard methods and purged with argon before use. Poly(9-vinylcarbazole) (PVK) with $M_n = 25,000$ – $50,000$ was purchased from Sigma–Aldrich and used without additional purification. Poly[3,4-(ethylenedioxy)thiophene]:poly-(styrenesulfonate) (PEDOT:PSS) (0.1–1.0 S/cm) and substrates with pixilated ITO anodes were supplied by Ossila. Column chromatography was carried out on Merck silica gel. Thin-layer chromatography (TLC) was performed on silica gel (Merck TLC Silica Gel 60). 9,10-Dibromoanthracene,^[31] 9,10-bis(trimethylsilyl)ethynylanthracene,^[32] 2,7-diiodofluorene,^[33] 2,7-diiodo-9,9-dibutylfluorene,^[34] 3,6-diiodocarbazole,^[35] 9-butyl-3,6-diiodocarbazole,^[36] and iodoarenes (**5**, **6**, **9**)^[37] were synthesized according to reported procedures with minor modifications, and were characterized by ¹H NMR spectroscopic analysis (see the Supporting Information for details).

Synthesis and Characterization

Sonogashira Cross-Coupling for the Synthesis of Anthracene Derivatives A1–A3. General Procedure: A solution of iodoarene (0.350 mmol, 2 equiv.) in THF (15 mL) was bubbled with argon and stirred for 10 min. After this time, the protected form of 9,10-diethynylanthracene **2** (65.2 mg, 0.176 mmol, 1 equiv.), Pd(PPh₃)₄ (40.5 mg, 0.035 mmol), and CuI (6.6 mg, 0.035 mmol) were added, and the resulting mixture was bubbled with argon for a further 10 min. TBAF (1 M in THF, 0.7 mL, 0.7 mmol) was then injected through the septum, and the mixture was stirred at room temperature for 24 h. The reaction mixture was filtered and the filtrate was evaporated under reduced pressure. The residue was purified by column chromatography.

9,10-Bis[7-(9H-carbazol-9-yl)-9,9-dibutylfluoren-2-yl]ethynylanthracene (A1): The crude product was purified by column chromatography (silica gel; hexane/dichloromethane, 4:1) and recrystal-

ized from hexane, to give **A1** (169 mg, 87 %) as an orange solid. ¹H NMR (400 MHz, CDCl₃): $\delta = 8.83$ (dd, $J_1 = 6.6$, $J_2 = 3.3$ Hz, 4 H), 8.20 (d, $J = 7.8$ Hz, 4 H), 7.99–7.97 (m, 2 H), 7.89–7.85 (m, 4 H), 7.79 (s, 2 H), 7.74 (dd, $J_1 = 6.7$, $J_2 = 3.2$ Hz, 4 H), 7.62–7.60 (m, 4 H), 7.50–7.44 (m, 8 H), 7.35–7.31 (m, 4 H), 2.18–2.06 (m, 8 H), 1.28–1.14 (m, 8 H), 0.90–0.77 (m, 20 H) ppm. ¹³C NMR (126 MHz, CDCl₃): $\delta = 153.0$, 151.4, 141.1, 140.9, 139.6, 137.0, 132.2, 131.2, 127.4, 126.9, 126.0, 126.0, 125.9, 123.5, 122.1, 121.8, 121.3, 120.5, 120.1, 120.0, 118.6, 109.8, 103.6, 87.1, 55.6, 40.1, 26.2, 23.1, 13.9 ppm. HRMS (ESI): m/z calcd. for C₈₄H₇₃N₂ [MH⁺] 1109.5774; found 1109.5778. C₈₄H₇₃N₂ (110.51): calcd. C 90.93, H 6.55, N 2.52; found C 89.83, H 6.58, N 2.10. Purity (DSC): 98.95 mol-%.

9,10-Bis[7-(N,N-diphenylamino)-9,9-dibutylfluoren-2-yl]ethynylanthracene (A2): The crude product was purified by column chromatography (silica gel; hexane/dichloromethane, 4:1) and recrystallized from hexane, to give **A2** (160.6 mg, 82 %) as a red solid. ¹H NMR (400 MHz, CDCl₃): $\delta = 8.78$ (dd, $J_1 = 6.6$, $J_2 = 3.3$ Hz, 4 H), 7.77–7.75 (m, 2 H), 7.70–7.67 (m, 8 H), 7.61 (d, $J = 8.2$ Hz, 2 H), 7.29–7.25 (m, 8 H), 7.15 (d, $J = 7.7$ Hz, 10 H), 7.05–7.02 (m, 6 H), 2.03–1.87 (m, 8 H), 1.21–1.07 (m, 8 H), 0.76–0.66 (m, 20 H) ppm. ¹³C NMR (126 MHz, CDCl₃): $\delta = 152.6$, 150.9, 147.9, 147.8, 141.8, 135.4, 132.1, 131.0, 129.2, 127.4, 126.8, 125.7, 124.1, 123.3, 122.8, 120.8, 120.8, 119.2, 118.9, 118.6, 104.0, 86.7, 55.2, 40.0, 26.1, 23.0, 13.9 ppm. HRMS (ESI): m/z calcd. for C₈₄H₇₇N₂ [MH⁺] 1113.6087; found 1113.6089. C₈₄H₇₇N₂ (1114.55): calcd. C 90.61, H 6.88, N 2.52; found C 89.72, H 6.97, N 2.72. Purity (DSC): 98.36 mol-%.

9,10-Bis[6-(9H-carbazol-9-yl)-9-butylcarbazol-3-yl]ethynylanthracene (A3): The crude product was purified by column chromatography (silica gel; hexane/dichloromethane, 1:1) and recrystallized from acetone, to give **A3** (154.7 mg, 88 %) as a brown solid. ¹H NMR (400 MHz, CDCl₃): $\delta = 8.77$ (dd, $J_1 = 6.6$, $J_2 = 3.3$ Hz, 4 H), 8.50 (d, $J = 1.2$ Hz, 2 H), 8.34 (d, $J = 1.2$ Hz, 2 H), 8.20 (d, $J = 7.8$ Hz, 4 H), 7.94 (dd, $J_1 = 8.5$, $J_2 = 1.5$ Hz, 2 H), 7.68–7.62 (m, 8 H), 7.55 (d, $J = 8.6$ Hz, 2 H), 7.43 (d, $J = 3.7$ Hz, 8 H), 7.33–7.29 (m, 4 H), 4.45 (t, $J = 7.2$ Hz, 4 H), 2.04–1.96 (m, 4 H), 1.56–1.48 (m, 4 H), 1.05 (t, $J = 7.4$ Hz, 6 H) ppm. ¹³C NMR (126 MHz, CDCl₃): $\delta = 141.9$, 141.0, 140.0, 132.0, 130.0, 129.6, 127.4, 126.6, 125.9, 125.8, 124.4, 123.5, 123.2, 122.7, 120.3, 119.8, 119.7, 118.5, 114.1, 110.1, 109.8, 109.4, 103.7, 85.4, 43.4, 31.3, 20.7, 14.0 ppm. HRMS (ESI): m/z calcd. for C₇₄H₅₅N₄ [MH⁺] 999.4427; found 999.4421. C₇₄H₅₅N₄ (1000.28): calcd. C 88.94, H 5.45, N 5.61; found C 87.78, H 5.43, N 5.56.

Measurements: NMR spectra were recorded in CDCl₃ with Bruker Advance 400 MHz (for ¹H NMR) or Bruker Advance 500 MHz (for ¹³C NMR) instruments. High-resolution mass spectrometry (HRMS) analysis was performed with a Waters Xevo G2 Q-TOF mass spectrometer (Waters Corporation) equipped with an ESI source operating in positive-ion modes. Full-scan MS data were collected from 100 to 1000 Da in positive ion mode with a scan time of 0.1 s. To ensure accurate mass measurements, data were collected in centroid mode and mass was corrected during acquisition using leucine enkephalin solution as an external reference (Lock-Spray™), which generated reference ion at m/z 556.2771 Da ([M + H]⁺) in positive ESI mode. The accurate mass and composition for the molecular ion adducts were calculated by using the MassLynx software (Waters) incorporated with the instrument. Elemental analyses were performed with a Vario EL III (Elementar, Germany). Thermogravimetric analysis (TGA) was carried out with a TG Pyris-1, Perkin–Elmer thermal analyzer with 10 °C/min in a stream of nitrogen (20 cm³/min) in the temperature range of 25–800 °C. Differential scanning calorimetry (DSC) was performed with a TA-DSC 2010 apparatus, under nitrogen atmosphere, using sealed aluminum pans with a heating rate 20 °C/min. UV/Vis absorption spectra of solu-

tions were recorded with a Perkin–Elmer Lambda Bio 40 UV/Vis spectrometer. Photoluminescence spectra of solutions were measured with a Varian Carry Eclipse spectrometer. UV/Vis spectra in the solid state as a film deposited on a glass substrate and as blends with poly(*N*-vinylcarbazole) on a glass substrate were recorded with a Jasco V570 UV-V-NIR Spectrometer. Photoluminescence spectra in the solid state were monitored with a Hitachi F-2500 spectrometer. The quantum yields (Φ_f) in chloroform solution, film, and blend were estimated by using the integrating sphere Avantes AvaSphere-80 with an FLS-980 Spectrophotometer (Edinburgh Instruments) under ambient temperature. Quantum yields measurements were performed by using the absolute method with the excitation wavelength with the most intense luminescence, in the case of solutions using chloroform as a blank. The active layer thickness was measured by atomic force microscopy (AFM) with a Topometrix Explorer TMX 2000.

Electrochemical measurements were carried out with an Eco Chemie Autolab PGSTAT128n potentiostat, glassy carbon electrode (diam. 2 mm), platinum coil, and silver wire as working, auxiliary, and reference electrode, respectively. Potentials are referenced with respect to ferrocene (Fc), which was used as the internal standard. Cyclic voltammetry experiments were conducted in a standard one-compartment cell, in CH₂Cl₂ (Carlo Erba, HPLC grade), under argon. 0.2 M Bu₄NPF₆ (Aldrich, 99 %) was used as the supporting electrolyte. The concentration of compounds was equal 10⁻⁶ mol/L. Deaeration of the solution was achieved by argon bubbling through the solution for about 10 min before measurement. All electrochemical experiments were carried out under ambient conditions. The current–voltage measurements were carried out with a Keithley 6517A source-measure unit. To collect electroluminescence (EL) spectra, the voltage was applied using a precise voltage supply (Gw Instek PSP-405) and the sample was fixed to an XYZ stage. Light from the OLED device was collected through a 30 mm lens, focused on the entrance slit (50 μm) of a monochromator (Shamrock SR-303i) and detected by using a CCD detector (Andor iDus 12305). Typical acquisition times were 10 seconds. The pre-alignment of the setup was done by using a 405 nm laser.

Film and Blend Preparation: Films and blends (15 wt.-% concentration of compound in PVK matrix) on glass substrates were prepared by spin coating (800 rpm, 60 s) from chloroform solution (10 mg/mL).

Device Preparation: Devices with two configurations: ITO:PEDOT:PSS/compound/Al and ITO:PEDOT:PSS/compound:PVK/Al containing 15 wt.-% of compound dispersed in PVK were fabricated. They were prepared on OSILLA substrates with pixilated ITO anodes, cleaned sequentially with detergent, deionized water, 10 % NaOH solution, water and 2-propanol in an ultrasonic bath. Substrates were covered with a PEDOT:PSS thin film (40 nm) by spin coating at 5000 rpm for 60 s and annealed for 15 min at 130 °C. The active layer was spin-coated on top of the PEDOT:PSS layer from chloroform solution (10 mg/mL) at 800 rpm for 60 s and dried at 100 °C for 10 min. Finally, an aluminum cathode was vacuum-deposited.

Theoretical Calculations: The calculations were carried out with Gaussian 09.^[38] Molecular geometries of the singlet ground state of the compounds were optimized in the gas phase at the B3LYP/6-311g⁺⁺ level of theory.^[39] For each compound, a frequency calculation was carried out, verifying that the obtained optimized molecular structure corresponds to an energy minimum, thus only positive frequencies were expected. The CIS(D) (single excitation configuration interaction with doubles correction) method^[40] was employed to calculate the electronic absorption spectra of the compounds in the dichloromethane solvent in PCM (Polarizable Contin-

uum Model) model. The contribution of a group (anthracene, fluorene, carbazole, Ph₂N-) to a molecular orbital was calculated by using Mülliken population analysis. GaussSum 3.0 program^[41] was used to calculate group contributions to the molecular orbitals and to prepare the partial density of states (DOS) spectra.

Acknowledgments

This work was supported by the National Centre for Research and Development, Poland (grant number PBS2/A5/40/2014). M. M. acknowledges a scholarship from the DoktoRIS project co-financed by the European Social. Calculations were carried out in the Wrocław Centre for Networking and Supercomputing (<http://www.wcss.wroc.pl>).

Keywords: Luminescence · Organic electronics · Thin films · Cross-coupling · Arenes · Heterogeneous catalysis

- [1] C. W. Tang, S. A. Vanslyke, *Appl. Phys. Lett.* **1987**, *51*, 913–915.
- [2] D. Y. Kondakov, J. R. Sandifer, C. W. Tang, R. H. Young, *J. Appl. Phys.* **2003**, *93*, 1108–1119.
- [3] B. Yang, S. K. Kim, H. Xu, Y. J. Park, H. Zhang, C. Gu, F. Shen, C. Wang, D. Liu, X. Liu, M. Hanif, S. Tang, W. Li, F. Li, J. Shen, J. W. Park, Y. Ma, *ChemPhysChem* **2008**, *9*, 2601–2609.
- [4] Y. Shirota, *J. Mater. Chem.* **2000**, *10*, 1–25.
- [5] M. S. Gong, H. S. Lee, Y. M. Jeon, *J. Mater. Chem.* **2010**, *20*, 10735–10746.
- [6] I. Cho, S. H. Kim, J. H. Kim, S. Park, S. Y. Park, *J. Mater. Chem.* **2012**, *22*, 123–129.
- [7] J. Y. Song, S. B. Lee, S. J. Lee, Y. K. Kim, S. S. Yoon, *Thin Solid Films* **2015**, *577*, 42–48.
- [8] A. Thangthong, D. Meunmart, N. Prachumrak, S. Jungsuttiwong, T. Keawin, T. Sudyoadsuk, V. Promarak, *Tetrahedron* **2012**, *68*, 1853–1861.
- [9] C. J. Chiang, A. Kimyonok, M. K. Etherington, G. C. Griffiths, V. Jankus, F. Turksyoy, A. P. Monkman, *Adv. Funct. Mater.* **2013**, *23*, 739–746.
- [10] K. Y. Lai, T. M. Chu, F. C. N. Hong, A. Elangovan, K. M. Kao, S. W. Yang, T. I. Ho, *Surf. Coat. Technol.* **2006**, *200*, 3283–3288.
- [11] H. W. Lee, H. J. Kim, Y. S. Kim, J. Kim, S. E. Lee, H. W. Lee, Y. K. Kim, S. S. Yoon, *Displays* **2015**, *39*, 1–5.
- [12] M. Aydemir, G. Haykir, A. Battal, V. Jankus, S. K. Sugunan, F. B. Dias, H. Al-Attar, F. Türksyoy, M. Tavasali, A. P. Monkman, *Org. Electron.* **2016**, *30*, 149–157.
- [13] Z. Zhao, X. Xu, X. Chen, X. Wang, P. Lu, G. Yu, Y. Liu, *Tetrahedron* **2008**, *64*, 2658–2668.
- [14] K. H. Lee, Y. S. Kwon, J. Y. Lee, S. Kang, K. S. Yook, S. O. Jeon, J. Y. Lee, S. S. Yoon, *Chem. Eur. J.* **2011**, *17*, 12994–13006.
- [15] T. Zhang, H. Dai, J. Li, *Displays* **2013**, *34*, 447–451.
- [16] L. Shi, Z. Liu, G. Dong, L. Duan, Y. Qiu, J. Jia, W. Guo, D. Zhao, D. Cui, X. Tao, *Chem. Eur. J.* **2012**, *18*, 8092–8099.
- [17] S. Sohn, M. J. Kim, S. Jung, T. J. Shin, H. K. Lee, Y. H. Kim, *Org. Electron.* **2015**, *24*, 234–240.
- [18] J. Y. Song, S. J. Lee, Y. K. Kim, S. S. Yoon, *Mater. Res. Bull.* **2014**, *58*, 145–148.
- [19] Z. Zhang, W. Jiang, X. Ban, M. Yang, S. Ye, B. Huang, Y. Sun, *RSC Adv.* **2015**, *5*, 29708–29717.
- [20] C. Lambert, S. Amthor, J. Schelter, *J. Phys. Chem. A* **2004**, *108*, 6474–6486.
- [21] C.-W. Wan, A. Burghart, J. Chen, F. Bergström, L. B.-A. Johansson, M. F. Wolford, T. G. Kim, M. R. Topp, R. M. Hochstrasser, K. Burgess, *Chem. Eur. J.* **2003**, *9*, 4430–4441.
- [22] Z. Zhao, S. Yu, L. Xu, H. Wang, P. Lu, *Tetrahedron* **2007**, *63*, 7809–7815.
- [23] J. W. Park, P. Kang, H. Park, H. Y. Oh, J. H. Yang, Y. H. Kim, S. K. Kwon, *Dyes Pigment.* **2010**, *85*, 93–98.
- [24] M. G. Shin, S. O. Kim, H. T. Park, S. J. Park, H. S. Yu, Y. H. Kim, S. K. Kwon, *Dyes Pigment.* **2012**, *92*, 1075–1082.
- [25] C. L. Devi, K. Yesudas, N. S. Makarov, V. J. Rao, K. Bhanuprakash, J. W. Perry, *Dyes Pigment.* **2015**, *113*, 682–691.
- [26] J. Shin, N. S. Kang, T. W. Lee, M. J. Cho, J. M. Hong, B. K. Ju, D. H. Choi, *Org. Electron.* **2014**, *15*, 1521–1530.

- [27] E. Schab-Balcerzak, M. Grucela-Zajac, M. Krompiec, H. Janeczek, M. Siwy, D. Sek, *Synth. Met.* **2011**, *161*, 2268–2279.
- [28] A. Plante, S. Palato, O. Lebel, A. Soldera, *J. Mater. Chem. C* **2013**, *1*, 1037–1042.
- [29] Y. Shirota, *J. Mater. Chem.* **2000**, *10*, 1–25.
- [30] P. Bujak, I. Kulszewicz-Bajer, M. Zagorska, V. Maurel, I. Wielgus, A. Pron, *Chem. Soc. Rev.* **2013**, *42*, 8895–8899.
- [31] D. Stern, N. Finkelmeier, D. Stalke, *Chem. Commun.* **2011**, *47*, 2113–2115.
- [32] Y. P. Ou, C. Jiang, D. Wu, J. Xia, J. Yin, S. Jin, G. A. Yu, S. H. Liu, *Organometallics* **2011**, *30*, 5763–5770.
- [33] S. H. Lee, T. Nakamura, T. Tsutsui, *Org. Lett.* **2001**, *3*, 2005–2007.
- [34] X. Ma, J. Jiao, J. Yang, X. Huang, Y. Cheng, C. Zhu, *Polymer* **2012**, *53*, 3894–3899.
- [35] Y. Wu, H. Guo, T. D. James, J. Zhao, *J. Org. Chem.* **2011**, *76*, 5685–5695.
- [36] W. Zeng, S. Liu, H. Zou, L. Wang, R. Beuerman, *J. Polym. Sci., Part A J. Polym. Sci., Part A: Polym. Chem.* **2010**, *48*, 4168–4177.
- [37] Y. Lin, Y. Chen, T. L. Ye, Z. K. Chen, Y. F. Dai, D. G. Ma, *J. Photochem. Photobiol. C* **2012**, *230*, 55–64.
- [38] M. J. Frisch, G. W. Trucks, H. B. Schlegel, G. E. Scuseria, M. A. Robb, J. R. Cheeseman, G. Scalmani, V. Barone, B. Mennucci, G. A. Petersson, H. Nakatsuji, M. Caricato, X. Li, H. P. Hratchian, A. F. Izmaylov, J. Bloino, G. Zheng, J. L. Sonnenberg, M. Hada, M. Ehara, K. Toyota, R. Fukuda, J. Hasegawa, M. Ishida, T. Nakajima, Y. Honda, O. Kitao, H. Nakai, T. Vreven, J. A. Montgomery Jr., J. E. Peralta, F. Ogliaro, M. Bearpark, J. J. Heyd, E. Brothers, K. N. Kudin, V. N. Staroverov, R. Kobayashi, J. Normand, K. Raghavachari, A. Rendell, J. C. Burant, S. S. Iyengar, J. Tomasi, M. Cossi, N. Rega, J. M. Millam, M. Klene, J. E. Knox, J. B. Cross, V. Bakken, C. Adamo, J. Jaramillo, R. Gomperts, R. E. Stratmann, O. Yazyev, A. J. Austin, R. Cammi, C. Pomelli, J. W. Ochterski, R. L. Martin, K. Morokuma, V. G. Zakrzewski, G. A. Voth, P. Salvador, J. J. Dannenberg, S. Dapprich, A. D. Daniels, Ö. Farkas, J. B. Foresman, J. V. Ortiz, J. Cioslowski, D. J. Fox, *Gaussian 09*, revision D.01, Gaussian, Inc., Wallingford CT, **2009**.
- [39] A. D. Becke, *J. Chem. Phys.* **1993**, *98*, 5648–5652.
- [40] M. Head-Gordon, R. J. Rico, M. Oumi, T. J. Lee, *Chem. Phys. Lett.* **1994**, *219*, 21–29.
- [41] cclib: A library for package-independent computational chemistry algorithms, see: N. M. O'Boyle, A. L. Tenderholt, K. M. Langner, *J. Comput. Chem.* **2008**, *29*, 839–45.

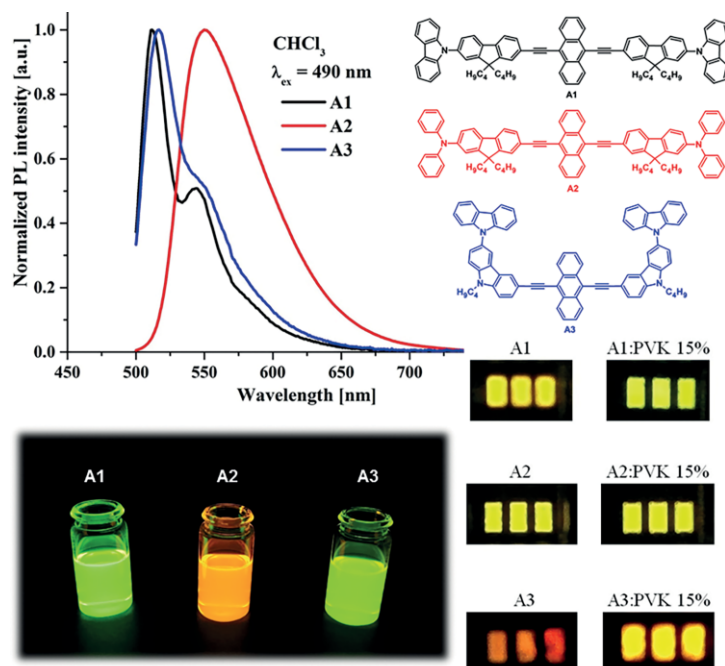
Received: April 28, 2016

Published Online: ■

Luminescence

A. Slodek, M. Filapek,
E. Schab-Balcerzak, M. Grucela,
S. Kotowicz, H. Janeczek, K. Smolarek,
S. Mackowski, J. G. Malecki,
A. Jedrzejowska,
G. Szafraniec-Gorol, A. Chrobok,
B. Marcol, S. Krompiec,
M. Matussek* 1–13

Highly Luminescence Anthracene Derivatives as Promising Materials for OLED Applications



Symmetrical anthracene derivatives with bulky units connected to the anthracene frame through an ethynyl bridge were synthesized and their electrochemical, photophysical, and electrical properties were character-

ized. The compounds were yellowish-orange emitters with high thermal stability, had excellent solubility in most organic solvents, and very high photoluminescence quantum yield in solution.

DOI: 10.1002/ejoc.201600532